High-Power Passively Mode-Locked Semiconductor Lasers

Reto Häring, Rüdiger Paschotta, Alex Aschwanden, Emilio Gini, François Morier-Genoud, and Ursula Keller, *Senior Member, IEEE*

***Abstract*—We have developed optically pumped passively mode-locked vertical-external-cavity surface-emitting lasers. We achieved as much as 950 mW of mode-locked average power in chirped 15–ps pulses, or 530 mW in 3.9–ps pulses with moderate chirp. Both lasers operate at a repetition rate of 6 GHz and have a diffraction-limited output beam near 950 nm. In continuous-wave operation, we demonstrate an average output power as high as 2.2 W. Device designs with a low thermal impedance and a smooth gain spectrum are the key to such performance. We discuss design and fabrication of the gain structures and, particularly, their thermal properties.**

***Index Terms*—Mode locking, pulse generation, semiconductor lasers, thermal effects in lasers.**

I. Introduction

FOR A LONG TIME, passively mode-locked semiconductor lasers were limited to relatively low output powers of typically only a few milliwatts. The main challenge for high mode-locked powers from a semiconductor laser is the need to maintain a single transverse mode. This requirement usually limits the usable mode area, and damage phenomena or gain saturation restrict the available pulse fluence. To increase the output power, several techniques have been used including flared waveguides [1], compound lasers with a tapered semiconductor amplifier section [2], and master-oscillator-power-amplifier systems with tapered [3] and inverse bow-tie amplifier geometries [4]. Such techniques increase the complexity of the system and are still currently limited to average powers well below 1 W.

In recent years, it has been discovered that semiconductor lasers with surface-emitting geometries allow for much larger mode areas, particularly when optical pumping is used, so that spatially homogeneous excitation is easily achieved [5]–[7]. An external cavity with properly designed fundamental mode size supports single-transverse-mode operation. In continuous-wave (CW) operation, output powers of more than 1 W in a diffraction-limited beam have been reported [8]. We have recently demonstrated for the first time [9], [10] that such lasers can be mode-locked with a semiconductor saturable absorber mirror (SESAM) [11]–[13] in the external cavity, which is a much more attractive technique than synchronous pumping [14], [15] with a mode-locked pump laser, or active mode locking [16], using a fast modulator in the cavity. While the power output of the first device was quite moderate, we soon significantly increased the output power to 0.2 W [17], and in this paper we describe how mode-locked output powers up to nearly 1 W are reached [18]. Even further significant increases of output power seem to be possible. It becomes clear that such lasers are becoming very attractive for applications like single-pass frequency conversion, printing or optical clocking of integrated circuits.

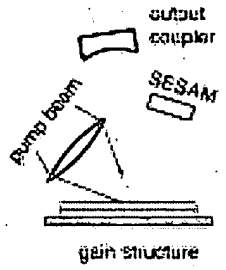

Fig. 1. Laser setup for a vertical-external-cavity surface-emitting laser (VECSEL) mode locked with a SESAM.

In Section II, we discuss the design and fabrication of high-power gain structures. In Section III-A, we derive a simple analytical model for the temperature rise in the active area, and determine the range of validity with a finite-element numerical simulation in Section III-B. Results for a high-power mode-locked device are presented in Section IV.

II. Setup and Device Structure

A. Laser Setup

Fig. 1 shows the mode-locked laser setup. The gain structure is used as a folding mirror so that the two ends of the standing-wave cavity can be used for output coupling and for the semiconductor saturable absorber mirror (SESAM), respectively. A curved output coupler determines a small mode area on the SESAM, such that the saturation energy of the absorber is lower than the saturation energy of the gain medium, as required for pulse formation [19], [20]. For a fixed pump spot size on the gain medium, we can vary the mode size on the absorber while keeping constant the mode size on the gain medium by properly adjusting the two arm lengths. The gain structure, which is discussed below, is pumped with a fiber-coupled diode array emitting at 808 nm. The output coupler has a transmission of 1.5% and a radius of curvature of 2.5 cm. The SESAM is based on a low-finesse antiresonant design consisting of a Bragg mirror with 25 pairs of GaAs/AlAs layers and a single quantum-well

Manuscript received November 31, 2002; revised May 31, 2002.

The authors are with the Institute of Quantum Electronics, Swiss Federal Institute of Technology, CH-8093 Zürich, Switzerland (e-mail: paschott@iqe.phys.ethz.ch).

Publisher Item Identifier 10.1109/JQE.2002.802111.

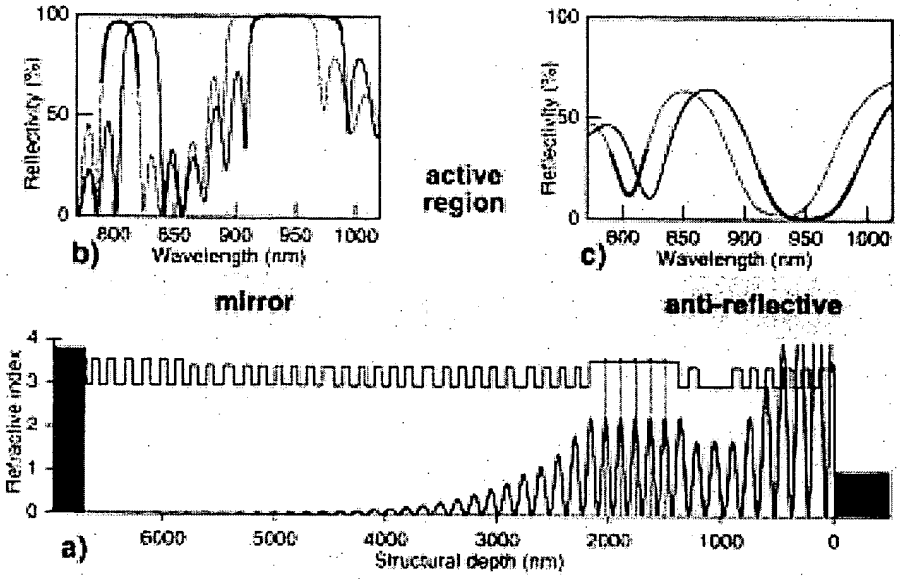

Fig. 2. Gain structure. (a) Refractive index profile through the structure with the standing wave pattern for the laser wavelength at 950 nm. Reflectivity spectra of (b) the mirror section and (c) the antireflective part are plotted for normal incidence (solid) and for an angle of 45° (dashed).

absorber, embedded in a GaAs spacer layer [12], [13]. The antiresonant Fabry–Perot is formed by the Bragg mirror, the $\lambda/2$ spacer layer with the embedded absorber and the Fresnel reflection from the top surface. The absorber is an 8-nm-thick $In_{0.15}Ga_{0.85}As$ quantum well grown with molecular beam epitaxy (MBE) at low temperature (450 °C). In the unsaturated state, the SESAM has reflection losses of 1.5%.

B. Design of the Gain Structure

The design of the gain structure is depicted in Fig. 2. It has to meet several requirements: 1) high reflectivity for the laser wavelength; 2) efficient pump absorption in the active region; 3) a large gain with a smooth spectral shape; 4) a large saturation fluence (as is favorable for pulse formation); and 5) a low thermal impedance for high-power performance. These demands are partly conflicting, and compromises have to be made. For example, a large gain could, in principle, be obtained by using a resonant structure with a partially reflecting mirror on top of the quantum wells, but such designs would lead to a narrow gain spectrum and to a small saturation fluence. Therefore, we use an antireflective structure (for the laser and the gain wavelength) above the amplifying quantum wells, obtaining a broad-gain bandwidth and larger saturation fluence but a reduced gain. A reasonably large gain is still achieved by using several (here, five) quantum wells. The numerically optimized antireflective structure consists of 14 layers of $Al_{0.2}Ga_{0.8}As$ and AlAs, covered with a 10-nm-thick cap layer of GaAs to prevent oxidation [Fig. 2(c)]. The residual reflectivities are 0.8% at the laser wavelength and 11% for the pump light at a 45° angle of incidence.

The pump radiation is absorbed with 85% efficiency in an active region of 0.8-μm thickness. This region contains the five 8.2-nm-thick $In_{0.15}Ga_{0.85}As$ quantum wells, which are placed in five subsequent antinodes of the standing-wave pattern. The carriers generated in the absorbing layers are efficiently transferred to the quantum wells and are trapped there. The total thickness of the active region is designed for resonance with the residual reflectivity of the antireflective structure for both the laser and pump wavelengths.

As the quantum wells are not lattice matched to the surrounding structure, strain relaxation (with detrimental effects on the efficiency of the gain structure) might occur when too many or too thick quantum wells are used. According to the studies of Wang *et al.* [21] on the critical layer thickness of multiple InGaAs quantum wells, our sequence should be stable. However, photoluminescence microscopy reveals some dark-line defects. This probably explains our observation that the device performance is strongly affected within an operation time on the order of 10 h. Preliminary tests with strain-compensated structures and a comparison with earlier devices [17] containing more quantum wells suggest indeed that the problem can be solved by proper balancing of the strain. This should also further improve the power efficiency.

For efficient pump absorption and minimized heating, the mirror structure has a high reflectivity not only for the laser light but also for the pump light [Fig. 2(b)]. The sequence is numerically optimized. Care is taken that no layer is far from $\lambda/4$ optical thickness, because this is found to result in designs with maximum tolerance against growth errors. The mirror has 62 layers, resulting in a reflectivity of 99.95% for the laser wavelength and 97% for the pump light.

The solid line in Fig. 3 is a plot of the measured reflectivity of the completely processed device. Especially for wavelengths longer than 950 nm, the agreement with the design (dotted) is very good, indicating good precision of the growth. We attribute the poorer match at 800–900 nm to the simplified model of the GaAs absorption and refractive index. The designed reflectivity

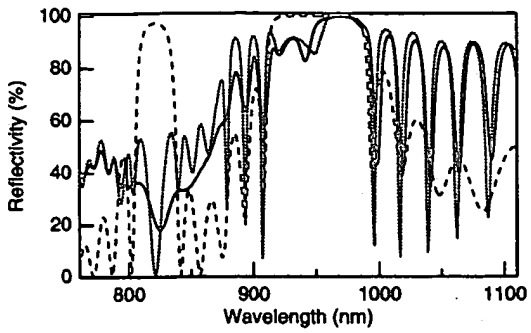

Fig. 3. Reflectivity spectra of the gain structure. Measured data of the soldered and etched structure are shown as a solid line. The designed reflectivity spectra are plotted for the complete structure (dotted) and for the mirror only (dashed).

of only the mirror structure is shown as a dashed line. For a 45° angle of incidence, the stop band around 830 nm shifts to the wavelength of the pump light at 808 nm.

C. Fabrication of the Gain Structure

The gain structure is grown with metal–organic chemical vapor deposition (MOCVD) on a 200-μm-thick (100) cut GaAs wafer. We use a growth temperature of 750 °C for the mirror and the antireflective structure and a reduced temperature of 610 °C for the active region.

As the generated heat has to be removed mainly through the back side, it is essential for high-power performance that the thickness of the whole semiconductor structure is as small as possible. Therefore, we want the gain structure and Bragg mirror not to rest on a thick semiconductor substrate but rather to be directly attached to a metallic heat sink. We achieve this with an epitaxial lift-off (ELO) technique. The principle is that we first grow three etch stop layers, followed by the gain structure and the Bragg mirror in reverse order, on the GaAs substrate. Then we solder a small dice of this structure to the copper heat sink and remove the GaAs substrate by selective etching. In the following, we present details of this technique.

For soldering the structure to the heat sink, we use a process similar to the one published by So *et al.* [22]. The epitaxial side of the wafer is metalized with 30 nm of titanium, 200 nm of platinum, 5000 nm of indium, and 100 nm of gold. The copper submount is lapped to have a planarity and roughness of $\approx$ 1 μm and is then coated with 30 nm of titanium, 200 nm of platinum, and 100 of nm gold. A 4 mm × 4 mm large dice of the processed wafer is pressed onto the copper heat sink with about 300 kPa. Soldering is done in vacuum at about $3 \cdot 10^{-5}$ mbar and $\approx$ 200 °C for 10 min.

The substrate is then removed by wet etching under a jet of H_2O_2:NH_4OH[23] stopping at a 300-nm-thick $Al_{0.85}Ga_{0.15}As$ layer. Hydrofluoric acid and H_2O_2:NH_4OH at pH 7.05 are used to remove the $Al_{0.85}Ga_{0.15}As$ and additional 20-nm GaAs and 70-nm AlAs etch stop layers. The surface quality is then characterized with atomic force microscopy. A 5 μm× 5 μm scan typically shows a roughness with a standard deviation of three monolayers. This quality of the surface is maintained over an aperture of 3 mm × 3 mm.

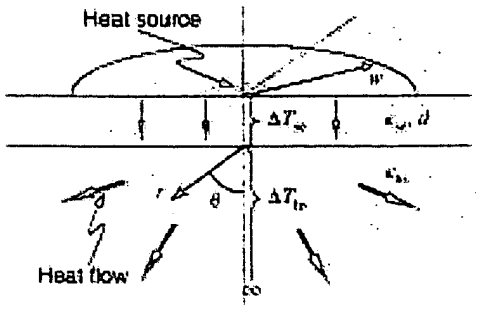

Fig. 4. Schematic of the parameters used in the analytical heat model. The parameters are described in the text.

III. Thermal Management

In this section, we investigate the thermal properties of an ELO gain structure. The reduced thickness of the semiconductor material leads to a nearly one-dimensional (1-D) heat flow into the heat sink and makes the device power scalable: for example, the output power can be doubled by applying twice the pump power to twice the mode area without raising the temperature of the gain structure. However, at one point this power scalability breaks down, namely, when the major part of the thermal impedance results from the heat sink (where the heat flow is not 1-D) and no longer from the semiconductor device.

A. Analytical Temperature Model

In Fig. 4, we show a schematic of the parameters we use in this model. We assume a thin semiconductor layer (gain structure with Bragg mirror) of thickness d with relatively low thermal conductivity κ_{se}. This layer is in intimate contact with a heat sink of larger thermal conductivity κ_{hs}. The heat source with total power P_{heat} has a Gaussian lateral distribution with the pump beam radius w_p ($1/e^2$ decay of the intensity) and a negligible thickness. With the pump beam radius w_p much larger than the layer thickness d, the heat flow into the heat sink is 1-D. The corresponding temperature rise in the center of the pumped spot relative to the interface is given by the heat flux times the thickness of the layer and divided by its thermal conductivity

$$\Delta T_{se} = 2\frac{P_{heat}d}{\pi w_p^2 \kappa_{se}}. \tag{1}$$

The heat sink is kept at a constant temperature at its lower boundary. However, for mathematical convenience we expand its size to infinity. This assumption might seem surprising but it proves to be a good approximation (errors < 10%) for a heat sink thicker than $3w_p$ (determined numerically). This is because most of the thermal impedance originates from the vicinity of the heat source, where the heat passes through the smallest cross section. The further heat flow can be calculated when mirroring the half space of the heat sink to achieve infinite boundary conditions. We use a spherical coordinate system with the heat source centered in the origin

$$\rho(r,\theta,\phi) = 2\frac{P_{heat}}{\pi w_p^2}\exp\left(-2\frac{r^2}{w_p^2}\right)\left(\frac{\delta\left(\theta-\frac{\pi}{2}\right)}{r}\right) \tag{2}$$

where δ is the delta function and the factor $1/r$ accounts for a heat source with constant thickness in lateral direction. The temperature elevation in the center of the heat source compared to the environment can be calculated by evaluating the Green's Function Solution Equation for the steady state [24], [25]

$$\Delta T_{\text{hs}} = 2\frac{1}{4\pi\kappa_{\text{hs}}}\int_V \frac{1}{r}\rho\, dV = \frac{P_{\text{heat}}}{\sqrt{2\pi}w_p\kappa_{\text{hs}}}. \tag{3}$$

The factor of 2 takes into account that the heat flow is only into half space.

Note that ΔT_{se} depends only on the heating intensity (in contrast to the heating power) while ΔT_{hs} increases with a larger pump spot but constant intensity. In order to distinguish two regimes, we define the parameter R as the ratio of the temperature drops in the semiconductor and the heat sink

$$R = \frac{\Delta T_{\text{hs}}}{\Delta T_{\text{se}}} = \sqrt{\frac{\pi}{8}}\frac{\kappa_{\text{se}}}{\kappa_{\text{hs}}}\frac{w_p}{d}. \tag{4}$$

For small pump spots, we have $R \ll 1$, which means that the temperature rise is mainly caused by the 1-D heat flow in the semiconductor. The condition for power scaling is fulfilled, and increasing the spot size proportional to the pump power leaves temperature, slope efficiency, and threshold intensity approximately unchanged. When we can provide enough pump power to keep the pump intensity constant, the achievable output power scales linearly with the spot area.

When $R > 1$, the thermal impedance is dominated by the three-dimensional heat flow in the heat sink. When the pump spot size is increased while maintaining the pump intensity, the temperature is raised. That does not mean necessarily that it is no longer possible to increase the output power by making the device larger (e.g., with a material system that shows good performance even at high temperatures). However, the detrimental effects of the increased temperature on the threshold intensity and slope efficiency will eventually limit the performance of a larger device.

We can define a critical radius w_{crit} where $R = 1$, so that a further increase of the pump spot size will make the thermal impedance of the heat sink surpass that of the semiconductor structure

$$w_{\text{crit}} = \sqrt{\frac{8}{\pi}}\frac{\kappa_{\text{hs}}\, d}{\kappa_{\text{se}}}. \tag{5}$$

Aiming for good performance in terms of both efficiency and maximum output power, we will choose the pump radius to be $\approx w_{\text{crit}}$. In most cases, the thickness of the structure and the thermal conductivity of the semiconductor material do not allow for much optimization. However, using a heat sink with a high thermal conductivity allows the critical radius to be increased. Since the critical radius depends linearly on the thermal conductivity, we find a quadratic dependence of the maximum output power on this thermal conductivity. For example, a copper heat sink with $\approx$10 times higher thermal conductivity than GaAs should allow 100 times more power to be extracted as compared with a gain structure on a thick GaAs substrate.

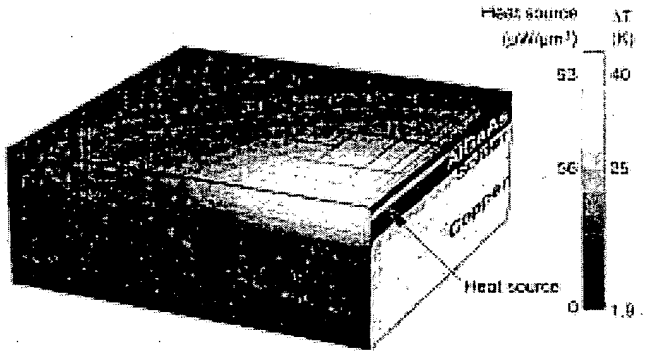

Fig. 5. Temperature distribution. The gain structure is soldered on a copper heat sink. The active area is heated with 512 mW on a pump spot with a 56.6-μm radius. Only the close surrounding of the heat source is shown, while the simulation expands much further.

B. Numerical Temperature Simulation

To examine the limits of validity of the analytical model, we simulated a device with a commercially available finite element software.[1] For the heat sink, we take a cube 5 mm in size cooled from the bottom (when the semiconductor layer is on top). The simulation is run with a 4.5-μm-thick Bragg mirror, a 1-μm-thick active region and a 1.5-μm-thick antireflective structure. Heat sink and semiconductor are joined with a 1-μm-thick solder junction. For the thermal conductivity we use 44 W/(K · m) for GaAs [26], 1000 W/(K · m) for diamond, 400 W/(K · m) for copper, and 30 W/(K · m) for the solder. For the gain structure, a superlattice of AlAs, $Al_{0.2}Ga_{0.8}As$ and GaAs, we take the value of $Al_{0.2}Ga_{0.8}As$ with 15 W/(K · m) [26].

An example of the temperature distribution simulated for a device on a copper heat sink with a pump spot of 56.6-μm radius and a heating power of 512 mW is shown in Fig. 5. The center of the heat source is at the front edge of the cube and only a small fraction of the simulated volume is depicted. We refine the grid until a further intersection of the finite elements has only a negligible effect on the result (0.2% for doubling the number of cells). The maximum temperature is reached in the center of the pumped spot, which is 41 K warmer than the bottom of the heat sink.

To compare the simulation with the analytical model we plot the temperature drops over the semiconductor and over the heat sink versus the pump beam radius (Fig. 6). The heating intensity is kept constant at 10.2 kW/cm^2. The model for a 1-D heat flow in the semiconductor is accurate to 10% for pump radii >40 μm. For smaller spot sizes, the cooling is more efficient because the heat spread in lateral direction has a significant contribution already in the semiconductor layer. The model for the three-dimensional heat flow in the heat sink is accurate to 10% for spot sizes <600 μm. For larger spots, the analytical model results in slightly lower temperatures because in the numerical model the heat flow is restricted by the sides of the heat sink. If we assume cooling from both the bottom and the sides of the copper heat sink in the numerical model, we get slightly lower temperatures than for the analytical model. For radii larger than the critical

[1]Solidis from ISE AG, Switzerland.

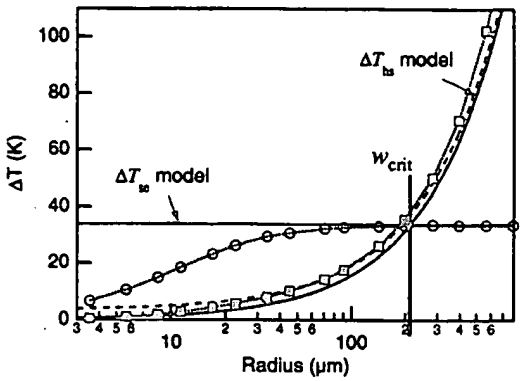

Fig. 6. Comparison of the analytical model with numerical simulations. The heating intensity is kept constant at 10.2 kW/cm² while the radius of the pump spot is increased. Results from the numerical simulation are plotted for the temperature drop over the semiconductor ΔT_{se} (circles) and over the heat sink ΔT_{hs} (squares). The analytical models are depicted as solid lines with the critical radius marked at the crossing point of the two lines. The dashed line also considers a 1-D heat flow in the solder junction.

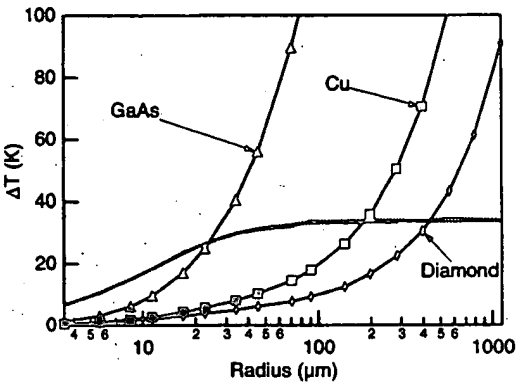

Fig. 7. Temperature drop for a constant pump intensity plotted versus pump spot radius. The temperature differences are measured over the AlGaAs Bragg mirror (dotted lines) and over the heat sink (solid lines with marker). Devices with a GaAs substrate (triangle) or directly mounted on a heat sink of copper (square) or diamond (rhombic) are simulated.

radius w_{crit}, the main contribution to the temperature elevation is caused by the heat sink. Power scaling by simply increasing the pump spot will then no longer work because the linear dependence of the temperature drop in the heat sink on the radius will eventually impair the efficiency of the laser. The critical radius is 213 μm for the configuration with 5-μm semiconductor material and a copper heat sink.

With further numerical tests, we come to the following conclusions. The actual shape of the heat sink has little influence on the result; e.g., a copper cube of 1000 times the volume results in a temperature increase of only $\approx$ 2% for a beam diameter of 400 μm. Cooling the heat sink from all sides rather than only from the bottom gives changes in the same range of a few percent. In contrast, by optically contacting a sapphire window to the front of the device for further heat removal [8], the temperature drop in the semiconductor structure can be reduced by $\approx$ 50%.

Fig. 7 shows simulation results for devices on a heat sink made of either diamond, copper, or a 330-μm-thick GaAs wafer on copper. The dotted lines are the temperature drops in the

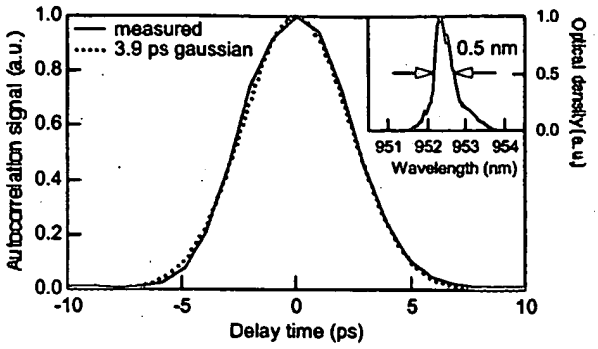

Fig. 8. Autocorrelation trace at 530 mW. The solid line depicts the measured data and the dotted line is a fit assuming a Gaussian pulse shape. Inset: the optical spectrum taken at a resolution of 0.1 nm.

semiconductor structure. As expected they are independent of the heat sink below and the three lines are covering. The solid lines with markers indicate the temperature drops in the heat sink. The critical radius obtained by these simulations are 24 μm for the device remaining on the substrate, 185 μm with a copper heat sink, and 435 μm using a diamond heat spreader.

IV. Mode-Locking Results

For the high-power mode-locking experiment, we use the setup described in Section II with a 30-W fiber-coupled diode array as the pump source. Up to 18 W of pump power on an elliptical spot with radii of 270 μm and 350 μm can be applied until we observe a roll-over of the output power. The heat sink is stabilized at a temperature of 3 °C. The most efficient pump absorption was achieved for an angle of 40°, where only 15% of the pump power is reflected. The cavity length of $\approx$ 25 mm determines the pulse repetition rate of $\approx$ 6 GHz. Fig. 8 shows the autocorrelation at an average output power of 530 mW. Assuming a Gaussian pulse shape, we calculate a pulse duration of 3.9 ps. The inset depicts the optical spectrum of the laser with a width of 0.5 nm (28 longitudinal modes) and a peak wavelength of 952 nm, taken with an optical spectrum analyzer with a resolution of 0.1 nm. The time–bandwidth product is 0.65, i.e., 1.5 times the Fourier limit of a Gaussian pulse. Fig. 9 shows the microwave spectrum of the laser output. The spectrum is free of noise down to the detection limit of -55 dBc at a resolution of 300 kHz and the inset shows a large frequency span with the harmonics of the 5.9533-GHz signal. The output beam is measured to be linearly polarized with a ratio better than 100 : 1. The M^2 values (measured with the knife-edge method) are < 1.05 in both transverse directions.

According to the analysis in Section III, for such a large pump spot, the thermal impedance is dominated by the heat sink. A smaller spot would allow a reduced temperature in the active area and thereby increase the efficiency of the laser. We used an aperture to clip off the outer parts of the pump beam and to achieve a pump spot with reduced radii of 160 μm $\times$ 206 μm. In a CW configuration (with the SESAM replaced with a high reflector) and using a piece of the wafer with higher efficiency, we can achieve 2.2 W of output power at the full available pump power of 15.8 W (see Fig. 10). In this case, the laser is allowed to run with a multi-mode transverse profile which has the best

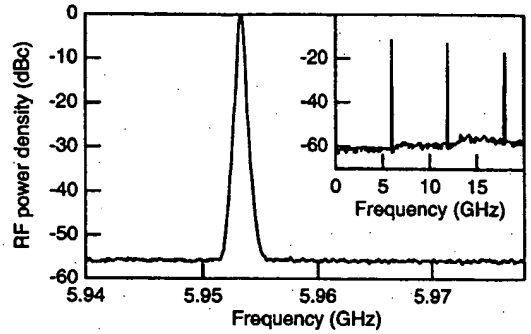

Fig. 9. Radio frequency spectrum of the laser output. The trace is measured at a resolution of 300 kHz. Inset: the signals at the harmonics of the repetition rate of 5.9533 GHz.

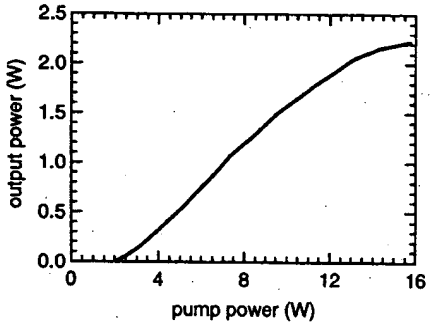

Fig. 10. Output power versus incident pump power in a CW configuration (without SESAM).

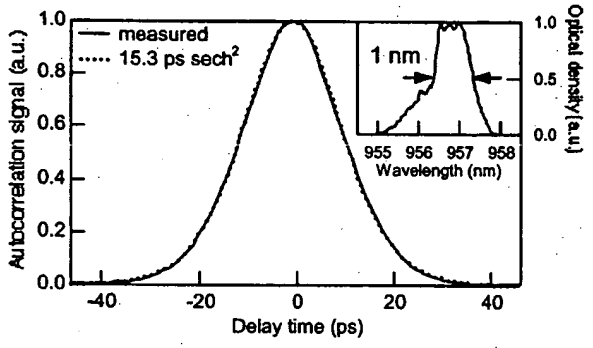

Fig. 11. Autocorrelation trace at 950 mW. Shown with a solid line are the measured data and the dotted line is a fit assuming a sech^2 pulse shape. Inset: optical spectrum taken at a resolution of 0.1 nm.

overlap with the pumped area. Forcing the cavity to operate on the fundamental transverse mode reduces the output by 35%. Introducing the saturable absorber for mode locking reduces the power by another 34%, resulting in an output power of 950 mW. The autocorrelation trace and the optical spectrum of this pulse are shown in Fig. 11. With a 15-ps pulse duration at a wavelength of 957 nm, the pulses are much longer, while the optical spectrum is even broader, indicating a strong chirp in this domain of operation.

The gain structure has a large variation of the group delay dispersion in the vicinity of the laser wavelength (the design has 0 fs^2 at 950 nm while a maximum of 2000 fs^2 is found at 956 nm). Due to the growth inhomogenity over the wafer, different spots on the wafer feature distinct dispersion properties and thereby lead to different pulse shapes. Proper control of the dispersion parameters in the cavity should allow significantly shorter pulses to be achieved [27].

The optical-to-optical efficiency of the CW laser is 14%. It is remarkable that when we pumped such structures with a smaller pump spot (using a high-brightness laser diode), we typically achieved significantly higher efficiencies of ≈30%. We hope to realize strongly improved efficiencies also with large pump spots by optimizing the designs for operation at higher temperatures and increasing the homogeneity and conversion efficiency of the samples, e.g., by using optimized strain compensation layers.

V. Conclusion

We have shown that VECSELs allow high-power performance of mode-locked semiconductor lasers at repetition rates of several gigahertz. So far we have demonstrated up to 950 mW of mode-locked average power at a 6-GHz repetition rate. The basis of such performance is a gain structure with a low thermal impedance and a smooth gain spectrum. We achieved this by soldering the structure to a copper heat sink and removing the substrate by selective etching. An analytical model of the thermal impedance of such a device has been established. Further improvements can be expected by a better understanding of the pulse formation and by the growth of more efficient structures. Even multiwatt level output with and pulse durations in the range of a picosecond or even below seem to be feasible.

References

[1] A. Mar, R. Helkey, W. X. Zou, D. B. Young, and J. E. Bowers, "High-power modelocked semiconductor lasers using flared waveguides," *Appl. Phys. Lett.*, vol. 66, pp. 3558–3560, June 1995.

[2] L. Goldberg, D. Mehuys, and D. Welch, "High power mode-locked compound laser using a tapered semiconductor amplifier," *IEEE Photon. Technol. Lett.*, vol. 6, p. 1070, 1994.

[3] A. Mar, R. Helkey, J. Bowers, D. Mehuys, and D. Welch, "Modelocked operation of a master oscillator power amplifier," *IEEE Photon. Technol. Lett.*, vol. 6, pp. 1067–1069, 1994.

[4] S. Gee, G. Alphonse, J. Connolly, and P. Delfyett, "High-power mode-locked external cavity semiconductor laser using inverse bow-tie semiconductor optical amplifiers," *IEEE J. Select. Topics Quantum Electron.*, vol. 4, pp. 209–215, 1998.

[5] J. V. Sandusky and S. R. J. Brueck, "A CW external-cavity surface-emitting laser," *IEEE Photon. Technol. Lett.*, vol. 8, pp. 313–315, Mar. 1996.

[6] M. Kuznetsov, F. Hakimi, R. Sprague, and A. Mooradian, "High-power (> 0.5 – W CW) diode-pumped vertical-external-cavity surface-emitting semiconductor lasers with circular TEM_{00} beams," *IEEE Photon. Technol. Lett.*, vol. 9, pp. 1063–65, Aug. 1997.

[7] ——, "Design and characteristics of high-power (> 0.5 – W CW) diode-pumped vertical-external-cavity surface-emitting semiconductor lasers with circular TEM_{00} beams," *IEEE J. Select. Topics Quantum Electron.*, vol. 5, pp. 561–573, May/June 1999.

[8] W. J. Alford, T. D. Raymond, M. H. Crawford, and A. A. Allerman, "High power (> 1 W), good beam quality surface-emitting semiconductor laser," *J. Opt. Soc. Amer.*, vol. B 19, no. 4, pp. 663–666, Apr. 2002.

[9] R. Häring, R. Paschotta, F. Morier-Genoud, U. Keller, A. Garnache, U. Oesterle, J. S. Roberts, S. Hoogland, S. Dhanjal, and A. C. Tropper, "Passively mode-locked diode-pumped surface-emitting semiconductor laser," presented at the Conf. Lasers and Electro-Optics CLEO'00, San Francisco, CA, 2000.

[10] S. Hoogland, S. Dhanjal, A. C. Tropper, S. J. Roberts, R. Häring, R. Paschotta, and U. Keller, "Passively mode-locked diode-pumped surface-emitting semiconductor laser," *IEEE Photon. Technol. Lett.*, vol. 12, pp. 1135–1138, Sept. 2000.
[11] U. Keller, D. A. B. Miller, G. D. Boyd, T. H. Chiu, J. F. Ferguson, and M. T. Asom, "Solid-state low-loss intracavity saturable absorber for Nd:YLF lasers: An antiresonant semiconductor Fabry-Perot saturable absorber," *Opt. Lett.*, vol. 17, pp. 505–507, Apr. 1992.
[12] U. Keller, K. J. Weingarten, F. X. Kärtner, D. Kopf, B. Braun, I. D. Jung, R. Fluck, C. Hönninger, N. Matuschek, and J. Aus der Au, "Semiconductor saturable absorber mirrors (SESAM's) for femtosecond to nanosecond pulse generation in solid-state lasers," *IEEE J. Select. Topics Quantum Electron.*, vol. 2, pp. 435–453, Sept. 1996.
[13] U. Keller, "Semiconductor nonlinearities for solid-state laser mode-locking and Q-switching," in *Nonlinear Optics in Semiconductors*, E. Garmire and A. Kost, Eds. Boston, MA: Academic, 1999, vol. 59, pp. 211–286.
[14] W. H. Xiang, S. R. Friberg, K. Watanabe, S. Machida, Y. Sakai, H. Iwamura, and Y. Yamamoto, "Sub-100 femtosecond pulses from an external-cavity surface-emitting InGaAs/InP multiple quantum well laser with soliton effect-compression," *Appl. Phys. Lett.*, vol. 59, p. 2076, Oct. 1991.
[15] W. Jiang and J. Bowers, "Ultrafast vertical cavity semiconductor lasers," in *Compact Sources of Ultrashort Pulses*, I. I. N. Duling, Ed. New York: Cambridge Univ. Press, 1995, pp. 208–273.
[16] M. A. Holm, P. Cusumano, D. Burns, A. I. Ferguson, and M. D. Dawson, "Mode-locked operation of a diode-pumped, external-cavity GaAs/AlGaAs surface emitting laser," presented at the Conf. Lasers and Electro-Optics, CLEO'99, Baltimore, MD, 1999.
[17] R. Häring, R. Paschotta, E. Gini, F. Morier-Genoud, H. Melchior, D. Martin, and U. Keller, "Picosecond surface-emitting semiconductor laser with > 200 mW average power," *Electron. Lett.*, vol. 37, pp. 766–767, June 2001.
[18] A. L. Aschwanden, R. Häring, R. Paschotta, E. Gini, F. Morier-Genoud, and U. Keller, "Passively mode-locked surface-emitting semiconductor laser with nearly 1 W average power," presented at the Conf. Lasers and Electro-Optics (CLEO '02), Long Beach, CA, 2002.
[19] G. H. C. New, "Modelocking of quasi-continuous lasers," *Opt. Commun.*, vol. 6, pp. 188–192, Oct. 1972.
[20] H. A. Haus, "Theory of mode locking with a slow saturable absorber," *IEEE J. Quantum Electron.*, vol. QE-11, pp. 736–746, Sept. 1975.
[21] C. A. Wang, S. H. Groves, J. H. Reinold, and D. R. Calawa, "Critical layer thickness of strained-layer InGaAs/GaAs multiple quantum wells determined by double-crystal X-ray diffraction," *J. Electron. Mater.*, vol. 22, pp. 1365–1368, Mar. 1993.
[22] W. W. So and C. C. Lee, "Fluxless process of fabricating In-Au joints on Copper substrates," *IEEE Trans. Comp. Packag. Technol.*, vol. 23, pp. 377–81, June 2000.
[23] J. J. LePore, "An improved technique for selective etching of GaAs and Ga(1-x)Al(x)As," *J. Appl. Phys.*, vol. 51, no. 12, pp. 6441–6442, Dec. 1980.
[24] P. M. Morse and H. Feshbach, *Methods of Theoretical Physics*. New York: McGraw-Hill, 1953.
[25] R. Paschotta, J. Aus der Au, G. J. Spühler, F. Morier-Genoud, R. Hövel, M. Moser, S. Erhard, M. Karszewski, A. Giesen, and U. Keller, "Diode-pumped passively mode-locked lasers with high average power," *Appl. Phys. B*, vol. 70, pp. S25–S31, June 2000.
[26] S. Adachi, "Properties of Aluminum Gallium Arsenide," in *Emis Datareviews Series*, 1 ed. London, U.K.: INSPEC, 1993, vol. 7, p. 323.
[27] R. Paschotta, R. Häring, A. Garnache, S. Hoogland, A. C. Tropper, and U. Keller, "Soliton-like pulse shaping mechanism in passively mode-locked surface-emitting semiconductor lasers," Appl. Phys. B, to be published.

Reto Häring was born in Basel, Switzerland, in 1971. He received the Diploma degree in experimental physics and the Ph.D. degree in 2001 from the Swiss Federal Institute of Technology (ETH), Zürich, Switzerland.

He joined the Institute of Quantum Electronics, ETH, in 1997. His research focuses on compact, diode-pumped, passively mode-locked and passively Q-switched lasers and on the design and characterization of semiconductor gain structures used for vertical-external-cavity surface-emitting lasers.

Rüdiger Paschotta was born in Tailfingen, Germany, in 1965. He received the Ph.D. degree in physics from the University of Konstanz, Konstanz, Germany, in 1994, for achievements in the fields of quantum optics and nonlinear optics.

From 1994 to 1997, he worked on fiber lasers and amplifiers at the Optoelectronics Research Centre at the University of Southampton, U.K. In 1997, he moved to the University of Paderborn, Germany, to work in nonlinear optics and integrated optics. Since November 1997, he has been conducting research on mode-locked lasers at the Swiss Federal Institute of Technology (ETH), Zürich, Switzerland. His scientific interests are currently focused on the physics of mode locking, optimization of mode-locked lasers for high powers or high repetition rates, the development of mode-locked surface-emitting semiconductor lasers, and high-power nonlinear frequency conversion.

Alexander Aschwanden was born in Zug, Switzerland, in 1974. He received the Diploma degree in experimental physics from the Swiss Federal Institute of Technology (ETH) Zürich, Switzerland.

At ETH, he joined the Institute of Quantum Electronics in 2000. His research is focused on the design and characterization of semiconductor saturable absorber mirrors for passively mode-locked lasers and on the design and characterization of semiconductor gain structures used for vertical-external-cavity surface-emitting lasers.

Emilio Gini was born in Davos, Switzerland, in 1961. He received the degree in physics and the Ph.D. degree in dry-etched InGaAsP/InP passive optical waveguide devices from the Swiss Federal Institute of Technology (ETH), Zürich, Switzerland, in 1986 and 1997, respectively.

In 1988, he joined the Institute of Quantum Electronics, ETH. He worked on the growth of III-V semiconductor compounds by LP-MOVPE and dry-etching techniques for the fabrication of optoelectronic integrated circuits. He participated in different European RACE, ESPRIT, ACTS, and COST projects, where he was involved in the development of low-loss optical waveguides with integrated corner mirrors and polarization-insensitive optical switches and modulators. He has written and coauthored about 40 scientific papers and conference contributions.

François Morier-Genoud was born in Geneva, Switzerland, in 1959. He received the degree in microtechnical engineering from the Technical University of Yverdon, Yverdon, Switzerland, in 1980.

In 1986, he joined the Swiss Federal Institute of Technology (EPFL), Zürich, Switzerland, as a Research Engineer in the field of III-V compounds semiconductors. He worked on molecular beam epitaxy and developed novel growth and characterization techniques. His research interests included the development of advanced light sources such as surface-emitting lasers, gain-coupled distributed feed back lasers and other devices for the optical networking and telecommunication systems. From 1996 to 2002, he worked at the sister university in Zürich (ETHZ) with the group of Prof. Keller on the development of saturable optical absorber materials. Since March 2002, he has been working as a Scientific Collaborator at the Institute of Quantum Electronics and Photonics, EPFL

Ursula Keller was born in Zug, Switzerland, in June 1959. She received the Diploma degree in physics from the Federal Institute of Technology (ETH) Zürich, Switzerland, in 1984 and the M.S. and Ph.D. degrees in applied physics from Stanford University, Stanford, CA, in 1987 and 1989, respectively. Her Ph.D. research involved optical probing of charge and voltage in GaAs integrated circuits and in low-noise ultrafast laser systems.

During 1984–1985, she researched optical bistability at Heriot-Watt University, Edinburgh, U.K. In 1989, she became a Member of Technical Staff (MTS) at AT&T Bell Laboratories, Holmdel, NJ, where she conducted research on photonic switching, ultrafast laser systems, and semiconductor spectroscopy. In 1993, she was appointed an Associate Professor, and in 1997, she became a Full Professor in the Physics Department at the Swiss Federal Institute of Technology (ETH), Zürich, Switzerland. During her first year at Stanford, she held a Fulbright Fellowship, and the following year, she was an IBM Predoctoral Fellow. Her current research interests are in ultrafast lasers, attosecond science, ultrafast spectroscopy, and novel devices for applications in optical information processing, communication, and medicine. She has published more than 170 journal papers and four book chapters and holds or has applied for 13 patents.

Prof. Keller was elected for the LEOS Distinguished Lecturer Award in 2000 for mode-locked solid-state lasers. She received the Carl Zeiss Research Award in 1998 for her pioneering work in novel modelocking and Q-switching techniques using semiconductor saturable absorber mirrors (SESAMs). She is a member of the Optical Society of America, the European Physical Society, the Swiss Physical Society, and the Swiss Academy of Technical Sciences.